

Extinguishment of Cup Burner Flames of Propane and the Aerosol Can Simulator Fuel by CF_3Br and C_2HF_5

Fumiaki Takahashi¹, Viswanath R. Katta², Gregory T. Linteris³, and Oliver C. Meier⁴

¹ Case Western Reserve University, Cleveland, OH 44106, USA

² Innovative Scientific Solutions, Inc., Dayton, OH 45440, USA

³ National Institute of Standards and Technology, Gaithersburg, MD 20899, USA

⁴ The Boeing Company, Seattle WA 98124, USA

Calculations have been performed for co-flow diffusion flames of propane and a propane-ethanol-water fuel mixture, prescribed for the Federal Aviation Administration (FAA) Aerosol Can Simulator, in the cup-burner configuration, with added CF_3Br and C_2HF_5 . The time-dependent, two-dimensional numerical code, which includes a detailed kinetic model (177 species and 2986 reactions) and diffusive transport, has predicted the minimum extinguishing concentration of agent and revealed the unique two-zone flame structure causing combustion enhancement by C_2HF_5 in zero gravity.

1. Introduction

Because of its destruction of stratospheric ozone, the use of the effective fire suppressant CF_3Br (Halon 1301) has been discontinued, except for certain critical applications such as the aircraft cargo-bay fire suppression. Recently, some halon replacement agents, including C_2HF_5 (HFC-125), have been evaluated in a mandated Federal Aviation Administration (FAA) aerosol can test (ACT) [1], in which a simulated explosion of an aerosol can, caused by a fire, must be suppressed by the agent. Unlike CF_3Br , the other agents created a higher over-pressure in the test chamber (when added at less than the inerting concentration) and thus failed the test. Similar combustion enhancement by various fire-extinguishing agents has been described in other experiments for certain conditions.

Recent work [2, 3] employing thermodynamic equilibrium and perfectly stirred-reactor calculations (for premixed systems) indicated that higher overpressures in the FAA ACT might be due to higher heat release from reaction of the inhibitor itself. Nonetheless, the fire-extinguishing agents should still reduce the overall reaction rate and inhibit the reaction. For diffusion flames, however, the inhibition or combustion enhancement processes by halogenated agents are not yet fully understood. This paper extends previous work [4-10] on cup-burner flames to more realistic fuels and agents in zero-gravity to uncover essential physical and chemical processes.

2. Computational Method

A time-dependent, axisymmetric numerical code (UNICORN) [11, 12] solves the axial and radial (z and r) full Navier-Stokes momentum equations, continuity equation, and enthalpy- and species-conservation equations on a staggered-grid system. A clustered mesh system is employed to trace the gradients in flow variables near the flame surface. The thermo-physical properties such as enthalpy, viscosity, thermal conductivity, and binary molecular diffusion of all of the species are calculated from the polynomial curve fits developed for the temperature range

300 - 5000 K. Mixture viscosity and thermal conductivity are then estimated using the Wilke and Kee expressions, respectively. Molecular diffusion is assumed to be of the binary-diffusion type, and the diffusion velocity of a species is calculated using Fick's law and the effective-diffusion coefficient of that species in the mixture. A simple radiation model based on the optically thin-media assumption was incorporated into the energy equation. Only radiation from CH_4 , CO , CO_2 , and H_2O was considered in the present study.

The finite-difference forms of the momentum equations are obtained using an implicit QUICKEST scheme [11], and those of the species and energy equations are obtained using a hybrid scheme of upwind and central differencing. At every time-step, the pressure field is accurately calculated by solving all of the pressure Poisson equations simultaneously and utilizing the LU (Lower and Upper diagonal) matrix-decomposition technique. The boundary conditions are treated in the same way as that reported in earlier papers [4-10].

A comprehensive reaction mechanism was assembled. The four-carbon hydrocarbon mechanism of Wang and co-workers [13, 14] (111 species and 1566 one-way reactions) was employed, and detailed reactions of ethanol (5 species and 72 reactions) by Dryer and co-workers [15-17] were added. For CF_3Br inhibition, the bromine parts of the mechanism of Babushok et al. [18, 19] (10 additional species and 148 reactions) were added. Finally, a subset (51 species and 1200 reactions) of NIST HFC starting mechanism [20-21] was used for HFCs. The final chemical kinetics model (177 species, 2986 reactions) is integrated into the UNICORN code. Validation of the code was performed. The predicted extinction strain rates for propane-air opposing-jet diffusion flames (no agent) were within 7.5% of the measured values by Zegers et al. [22]. The fuel is propane or the ACT fuel gas mixture (volume fractions: C_3H_8 , 0.159; $\text{C}_2\text{H}_5\text{OH}$, 0.454; and H_2O , 0.387), and the agent is CF_3Br or C_2HF_5 added to "air" (21 % O_2 in N_2).

3. Results and Discussion

The flame-base region supports a trailing flame and controls the flame attachment and detachment processes [23]. Small variations in the agent mole fraction in the coflowing oxidizing stream (X_a) result in profound changes near the extinguishment limit. Figure 1 shows the calculated structure of a zero-gravity ($0g_n$) near-limit propane flame with agent (C_2HF_5) added at $X_a = 0.093$. The variables include the velocity vectors (\mathbf{v}), isotherms (T), and heat-release rate (\dot{q}). The flame base is already detached and lifted above the burner rim. The contours of the heat-release rate showed a peak reactivity spot (i.e., the *reaction kernel* [23]) at the height from the burner rim, $z_k = 10.9$ mm. The chain radical species as well as heat diffused back against the incoming flow at the flame base (edge), thus promoting vigorous reactions to form the reaction kernel.

Figure 2 shows the radial and axial variations of the species mole fractions (X_i), temperature, and

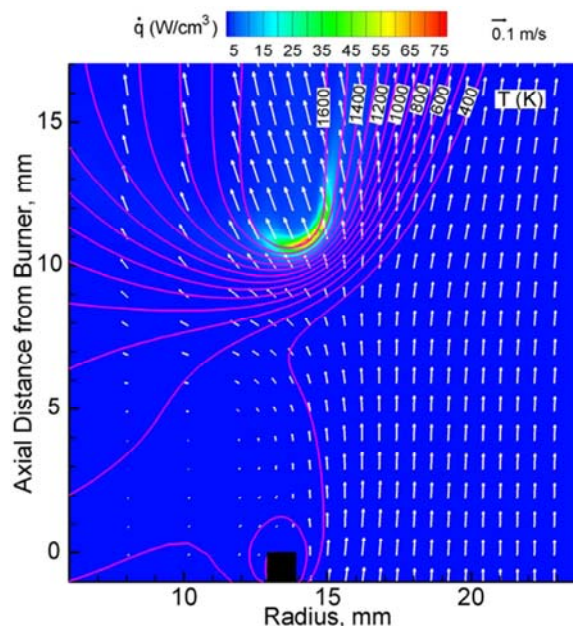


Fig. 1. Calculated structure of a $0g_n$ C_3H_8 flame in air with added C_2HF_5 at $X_a=0.093$.

heat-release rate (HRR) crossing the reaction kernel of the flame at $X_a=0.093$. The general trend in the radial plot at $z = 10.9$ mm (Fig. 2a) is similar to that in the methane flame with added nitrogen [10], except that X_{CO} was much larger, X_{H_2O} was much smaller, and there are broad and large concentrations of HF, CF_2O , and minor fluorinated intermediates on both fuel and oxidizer sides. The heat-release rate peak was formed on the oxidizer side. The axial plot (Fig. 2b) revealed the premixed-like nature of the unique flame-base structure. At increasing axial distances along $r = 14.4$ mm, the mole fractions of the reactants (C_3H_8 , O_2 , and C_2HF_5) decreased, intermediate species and chain radicals (H, O, and OH) peaked, the temperature increased, the heat-release rate peaked, and the final products (CO_2 , HF, and CF_2O) were formed. Surprisingly, H_2O and H_2 formed by hydrocarbon- O_2 reaction were completely converted to HF and CF_2O . Notice that X_O was much higher than X_H and X_{OH} .

Figure 3 shows the radial variations of calculated variables crossing the trailing flame at $z = 15.9$ mm ($z_k + 5$ mm). At this height, the flame structure is characterized by two zones (inner and outer) as is evident from two heat-release rate peaks. In the inner zone ($11 < r < 15$ mm), T , X_H , X_O , and X_{OH} peaked, and hydrocarbon fuel fragments and, more importantly X_{H_2O} and X_{H_2} from the fuel side, diminished, unlike in a neat diffusion flame without a halogenated agent [10]. As the case at the reaction kernel, X_O peak was much larger than X_H and X_{OH} and penetrated into the outer zone. In the outer zone ($15 < r < 18$ mm), the agent (C_2HF_5) from the air side decomposed and diminished, the mole fractions of many fluorinated species (CF_2O , CF_4 , CF_3-CF_3 , CHF_3 , etc.) peaked.

Figure 4 shows the radial variations of the calculated production(+)/consumption (-) rates (Fig. 4a) and heat-release rates (Fig. 3b) of species i crossing the trailing flame at $z = 15.9$ mm. In the inner zone, H_2 , H_2O , CO, O_2 , F, and CF_2O were consumed, HF and CO_2 were

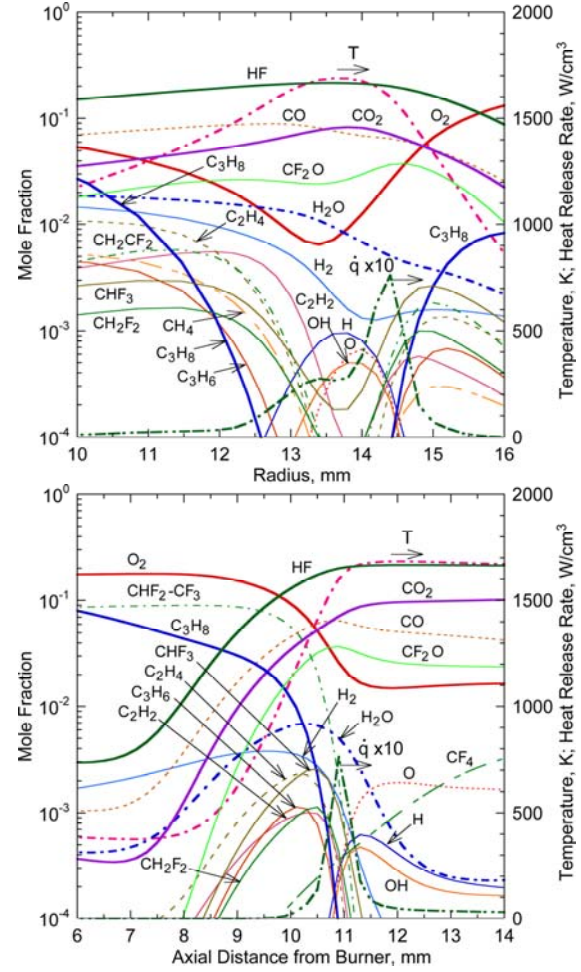


Fig. 2 Calculated structure through the reaction kernel for a $0g_n$ C_3H_8 flame in air with C_2HF_5 at $X_a=0.093$. (a) Radial ($z=10.9$ mm) and (b) axial ($r=14.4$ mm) variations.

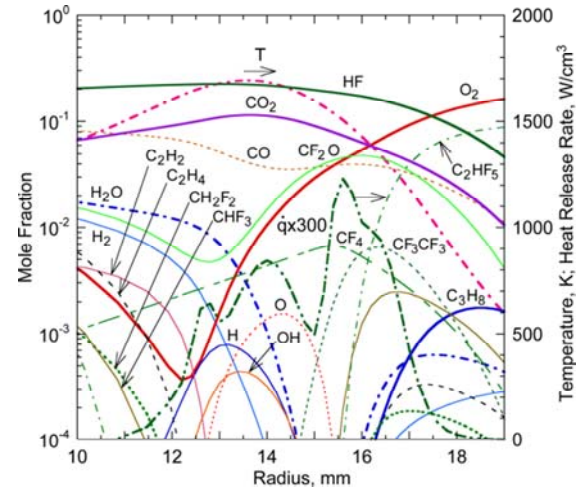


Fig. 3 Calculated structure across the trailing flame for a $0g_n$ C_3H_8 flame in air with C_2HF_5 at $X_a=0.093$ ($z_k=15.9$ mm).

formed, and the chain radicals (H, O, and OH) were formed and consumed depending on the radial location. In the outer zone, C_2HF_5 , and O_2 were consumed, HF, CF_2O , and CO were formed, and F was formed on the fuel side and consumed on the air side. The major contributors to the overall heat-release rate (Fig. 4b) were the formation of CO_2 and HF in the inner zone and CF_2O and HF in the outer zone.

Figure 5 shows the maximum heat-release rate of each elementary step crossing the reaction kernel and the trailing flame ($z = 10.9$ mm and 15.9 mm, respectively). At the reaction kernel, many steps for CF_2O and HF (and CO_2) formation contributed to overall HRR, while in the trailing flame, HF formation from H_2O and H_2 in addition to the CO_2 formation (inner zone) and the HF from C_2HF_5 and the CF_2O from CF_3 (outer zone) were the main contributors.

The structure of the ACT fuel flame (not shown) was very similar to that of the propane flame, except for generally larger X_{H_2O} and $X_{C_2H_5OH}$, and smaller $X_{C_3H_8}$ because of the initial fuel composition.

Figure 6 shows the effects of the agent volume fraction in the coflowing oxidizer on the calculated axial (z_k) and radial (r_k) positions of the reaction kernel from the burner exit on the axis in both propane and ACT fuel flames with added CF_3Br or C_2HF_5 . As X_a was increased, the axial standoff distance of the reaction kernel increased steeply as the calculated minimum extinguishing concentration (Table 1) approached, while the radial location remained nearly constant.

Table 1 Minimum Extinguishing Concentrations

Fuel	C_3H_8		ACT Fuel	
	CF_3Br	C_2HF_5	CF_3Br	C_2HF_5
Agent	CF_3Br	C_2HF_5	CF_3Br	C_2HF_5
MEC (%)	2.54	9.7	2.08	11.2

Figure 7 shows the temperature, heat-release rate, and a ratio of the heat-release rate and the total velocity at the reaction kernel. As X_a was

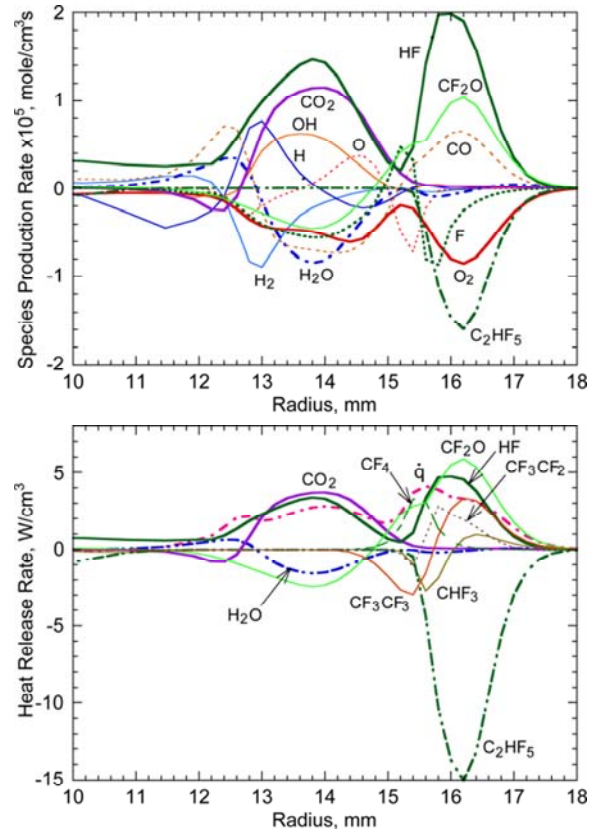


Fig. 4 (a) Species production rates, and (b) species and total heat-release rates crossing the trailing flame for a $0g_n$ C_3H_8 flame in air with C_2HF_5 at $X_a=0.093$ ($z=15.9$ mm).

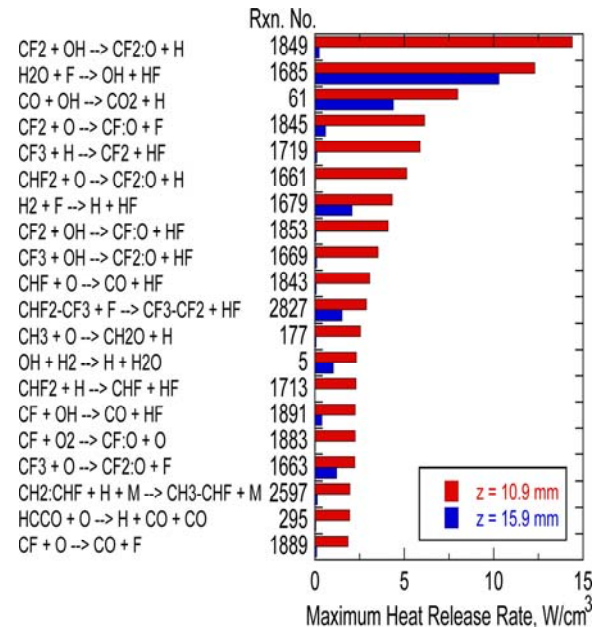


Fig. 5 Maximum heat flux of each step across the reaction kernel and trailing flame for a $0g_n$ C_3H_8 flame in air with C_2HF_5 at $X_a=0.093$.

increased for both fuels and both agents, the reaction kernel weakened (lower \dot{q}_k), but the flame stabilized at higher T_k . The quantity $\dot{q}_k/|\mathbf{v}_k|$ (which relates to a ratio of the residence time and the reaction time, i.e., local Damkhöler number, at the reaction kernel [23]) decreased mildly, stayed nearly constant over a wide range, and decreased rapidly (just before lifted off) to a minimum level (3-4), which was comparable to the chemically passive agents [9, 10]. The reaction kernel lifted gradually downstream to seek a balance until blew out eventually.

Figure 8 shows the maximum temperature (T_{\max}) in the trailing diffusion flame, the total heat-release rate (\dot{q}_{total}) integrated over the entire flame, and the flame base region ($\dot{q}_{<z_k+3 \text{ mm}}$) only. Unlike chemically passive agents [9, 10], which work thermally to reduce the flame temperature by dilution, the maximum flame temperature remained constant (or increased slightly) over an entire range of X_a varied until lifting. There was a striking difference between CF_3Br and C_2HF_5 in \dot{q}_{total} over the entire flame. \dot{q}_{total} decreased (i.e., inhibition) with added CF_3Br , whereas it increased (i.e., combustion enhancement) with added C_2HF_5 . On the other hand, for both fuels and both agents, $\dot{q}_{<z_k+3 \text{ mm}}$ was nearly constant. Thus, the combustion enhancement occurred only in the trailing flame. In fact, $(\dot{q}_{\text{total}} - \dot{q}_{<z_k+3 \text{ mm}})$ doubled with added C_2HF_5 (at $X_a \approx 0.1$). Although the volumetric heat-release rate in the trailing flame was an order-of-magnitude smaller than the peak \dot{q}_k , integration over the entire trailing flame zone made the total value much larger. This result suggests the significant implication that even if the reaction kernel, with premixed-like flame structure, is weakened by halogenated agent addition toward the flame stability limit, the trailing flame can burn more reactants (including the agent itself) because of the additional heat release to form HF and CF_2O in the aforementioned two-zone flame structure.

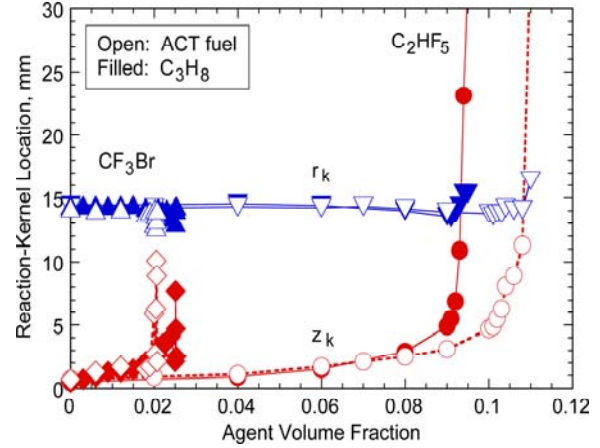


Fig. 6 Calculated reaction kernel coordinates of $0g_n$ C_3H_8 and ACT fuel flames in air with added agent.

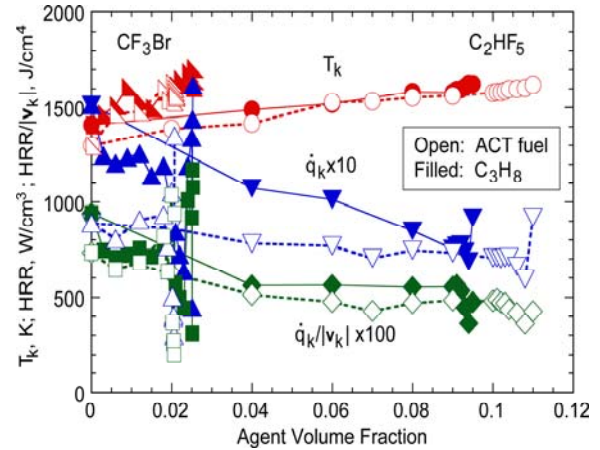


Fig. 7 Calculated heat-release rate, and its ratio to total velocity at the reaction kernel of $0g_n$ C_3H_8 and ACT fuel flames in air with added agent.

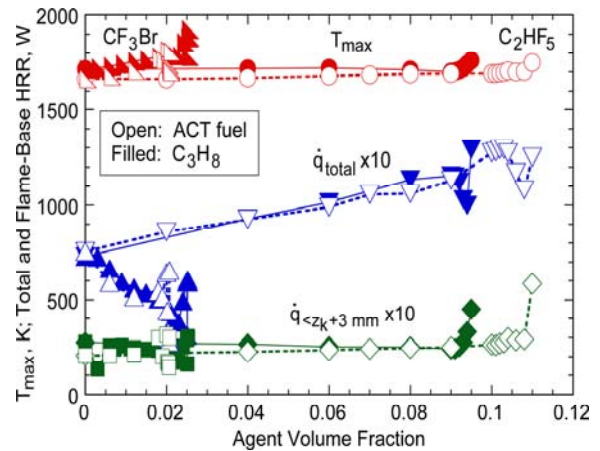


Fig. 8 Calculated maximum temperature, total heat release rate integrated over an entire flame, and the base region of $0g_n$ C_3H_8 and ACT fuel flames in air with added agent.

4. Conclusions

Addition of CF_3Br or C_2HF_5 to the oxidizer weakened the flame attachment point (reaction kernel) at the flame base, thereby inducing the detachment, lifting, and blowout extinguishment eventually. Unlike chemically passive agents studied previously, the calculated maximum flame temperature in the trailing diffusion flame remained constant (or increased slightly) and the reaction kernel temperature increased, as a result of additional heat release from the inhibitor itself. Nevertheless, CF_3Br successfully inhibited the reaction and reduced the overall total heat release. By contrast, the C_2HF_5 addition resulted in the combustion enhancement (increased total heat release) in the unique two-zone structure of the trailing flame: inner zone where CO_2 was formed from CO , and HF from H_2O and H_2 ; and outer zone where CF_2O and HF were formed from C_2HF_5 and its fluorinated fragments.

Acknowledgments

This work was supported by The Boeing Company.

References

- [1] J.W. Reinhardt, Behavior of Bromotrifluoropropene and Pentafluoroethane When Subjected to a Simulated Aerosol Can Explosion, DOT/FAA/AR-TN04/4, 2004.
- [2] G.T. Linteris, F. Takahashi, V.R. Katta, H. Chelliah, Thermodynamic analysis of suppressant-enhanced overpressure in the FAA Aerosol Can Simulator, in *Fire Safety Science—Proceedings of the Tenth International Symposium*, 2011.
- [3] G.T. Linteris, V.R. Katta, F. Takahashi, H. Chelliah, O. Meier, Stirred-Reactor Calculations to Understand Unwanted Combustion Enhancement by Potential Halon Replacements, *Combust. Flame* (2012), in press.
- [4] V.R., Katta, F. Takahashi, G.T. Linteris, *Combustion and Flame* 137 (2004) 506-522.
- [5] G.T. Linteris, V.R., Katta, F. Takahashi, *Combustion and Flame* 138 (2004) 78-96.
- [6] V.R. Katta, F. Takahashi, G.T. Linteris, *Combustion and Flame* 144 (2006) 645-661.
- [7] G.T. Linteris, F. Takahashi, V.R., Katta, *Combustion and Flame* 149 (2007) 91-103.
- [8] F. Takahashi, G.T. Linteris, V.R., Katta, *Proceedings of the Combustion Institute* 31 (2007) 2721-2729.
- [9] F. Takahashi, G.T. Linteris, V.R., Katta, *Combustion and Flame* 155 (2008) 37-53.
- [10] F. Takahashi, G.T. Linteris, V.R., Katta, *Proceedings of the Combustion Institute* 33 (2011) 2531-2538.
- [11] V.R., Katta, L.P. Goss, W.M. Roquemore, *AIAA Journal* 32 (1994) 84.
- [12] W.M. Roquemore, V.R., Katta, *Journal of Visualization* 2 (2000) 257-272.
- [13] H. Wang, X. You, K.W. Jucks, S. G. Davis, A. Laskin, F. Egolfopoulos, C. K. Law, USC Mech Version II. High-temperature combustion reaction model of $\text{H}_2/\text{CO}/\text{C}_1\text{-C}_4$ compounds, available at <http://ignis.usc.edu/USC_Mech_II.htm>, University of Southern California, Los Angeles, CA, 2007.
- [14] D.A. Sheen, X.Q. You, H. Wang, T. Lovas, *Proceedings of the Combustion Institute* 32 (2009) 535-542.
- [15] J. Li, A. Kazakov, F.L. Dryer, *Journal of Physical Chemistry A* 108 (2004) 7671-7680.
- [16] J. Li, A. Kazakov, M. Chaos, F.L. Dryer, Chemical Kinetics of Ethanol Oxidation, US Sections/The Combustion Institute Meeting (2007).
- [17] J. Li, A. Kazakov, F.L. Dryer, *Int. Journal of Chemical Kinetics* 33 (2001) 859-867.
- [18] V.I. Babushok, D.R.F. Burgess, W. Tsang, A.W. Miziolek, Simulation studies on the effects of flame retardants on combustion processes in a plug reactor, In: *Halon Replacements*, 1995, pp. 275-288.
- [19] V.I. Babushok, T. Noto, D.R.F. Burgess, A. Hamins, W. Tsang, *Combustion and Flame* 107 (1996) 351-367.
- [20] D. Burgess, M.R. Zachariah, W. Tsang, P.R. Westmoreland, *Prog. Energy Combust. Sci.* 21 (1995) 453-529.
- [21] D. Burgess, M.R. Zachariah, W. Tsang, P.R. Westmoreland, Thermochemical and chemical kinetic data for fluorinated hydrocarbons, NIST Technical Note 1412, 1995.
- [22] E. J. P. Zegers, B.A. Williams, E.M. Fisher, J.W. Fleming, R.S. Sheinson, *Combustion and Flame* 121 (2000) 471-487.
- [23] F. Takahashi, V.R. Katta, *Proceedings of the Combustion Institute* 28 (2000) 2071-2078.